RADIATION RESEARCH **164**, 194–201 (2005)
0033-7587/05 $15.00

Monte Carlo Simulation of Base and Nucleotide Excision Repair of Clustered DNA Damage Sites. II. Comparisons of Model Predictions to Measured Data

V. A. Semenenko and R. D. Stewart[1]

Purdue University, School of Health Sciences, West Lafayette, Indiana 47907-2051

Semenenko, V. A. and Stewart, R. D. Monte Carlo Simulation of Base and Nucleotide Excision Repair of Clustered DNA Damage Sites. II. Comparisons of Model Predictions to Measured Data. *Radiat. Res.* 164, 194–201 (2005).

Clustered damage sites other than double-strand breaks (DSBs) have the potential to contribute to deleterious effects of ionizing radiation, such as cell killing and mutagenesis. In the companion article (Semenenko *et al.*, *Radiat. Res.* 164, 180–193, 2005), a general Monte Carlo framework to simulate key steps in the base and nucleotide excision repair of DNA damage other than DSBs is proposed. In this article, model predictions are compared to measured data for selected low- and high-LET radiations. The Monte Carlo model reproduces experimental observations for the formation of enzymatic DSBs in *Escherichia coli* and cells of two Chinese hamster cell lines (V79 and xrs5). Comparisons of model predictions with experimental values for low-LET radiation suggest that an inhibition of DNA backbone incision at the sites of base damage by opposing strand breaks is active over longer distances between the damaged base and the strand break in hamster cells (8 bp) compared to *E. coli* (3 bp). Model estimates for the induction of point mutations in the human hypoxanthine guanine phosphoribosyl transferase (*HPRT*) gene by ionizing radiation are of the same order of magnitude as the measured mutation frequencies. Trends in the mutation frequency for low- and high-LET radiation are predicted correctly by the model. The agreement between selected experimental data sets and simulation results provides some confidence in postulated mechanisms for excision repair of DNA damage other than DSBs and suggests that the proposed Monte Carlo scheme is useful for predicting repair outcomes.

INTRODUCTION

Although double-strand breaks (DSBs) are widely accepted as the most critical form of DNA damage produced by ionizing radiation, it has long been suggested that a broader class of damage may be responsible for the observed biological effects. Such damage sites are composed of several single-nucleotide modifications within one or two helical turns of the DNA (10–20 bp) and have been termed multiply damaged sites (*1, 2*) or clustered damages (*3*). The existence of clustered damage other than DSBs was predicted in modeling studies (*3, 4*) and has now been confirmed experimentally (*5, 6*). DNA lesions that constitute clustered damage sites may include modified bases, AP (apurinic/apyrimidinic) sites, and strand breaks, all of which are repaired by base excision repair (BER) (*7*). The nucleotide excision repair (NER) pathway can also repair AP sites and certain types of base damage (*8*).

Several experiments provide evidence that clustered damage sites can be converted into DSBs as a result of unsuccessful excision repair of radiation-induced DNA damage. We refer to these DSBs as enzymatic DSBs to distinguish them from the prompt DSBs that are formed directly by ionizing radiation. Bonura *et al.* (*9*) demonstrated that additional DSBs may arise in an *E. coli* strain deficient in the gap-filling synthesis step of excision repair after γ-ray exposure. A postirradiation increase in DSB yields has also been observed in Chinese hamster cells (*10, 11*) and in plasmid DNA incubated with *E. coli* cell extracts (*12*). Studies by Harrison *et al.* (*13*) with oligonucleotide DNA sequences demonstrate that BER enzyme complexes from *E. coli* can convert a base damage (8-oxoG) opposite a strand break into a DSB. Normal bacterial cells are more radiosensitive than mutants lacking DNA glycosylases (*14*). This result is attributed to aborted BER of closely spaced lesions within clustered damage sites that leads to the formation of potentially lethal DSBs. Although results obtained in earlier studies (*9–12*) may be prone to artifacts caused by detection of heat-labile sites (*15, 16*), two laboratories have recently provided compelling evidence for the formation of enzymatic DSBs in Chinese hamster ovary xrs5 cells (*17*) and human lymphoblastoid TK6 cells (*18*) after exposure to ionizing radiation.

The misrepair of clustered damage also has the potential to cause local changes in the DNA sequence, such as base substitutions, small deletions and insertions. Such events

[1] Author to whom correspondence should be addressed at Purdue University, School of Health Sciences, 550 Stadium Mall Drive, West Lafayette, IN 47907-2051; e-mail: trebor@purdue.edu

are classified as point mutations in mutagenesis studies (*19*). Weinfeld *et al.* (*20*) hypothesized that, when a cluster is repaired, a polymerase may need to insert a nucleotide opposite a lesion present in the other strand, which may have mutagenic consequences. Ward *et al.* (*21*) suggested that aberrant repair of clustered damage may result in enzymatic DSBs which, if they occur within an exon of the gene, may be converted into point mutations.

In the companion article (*22*), we proposed for the first time a general Monte Carlo framework to simulate key steps in the base and nucleotide excision repair of DNA damage other than DSBs. The quantitative implications of alternative hypotheses regarding the postulated repair mechanisms have been investigated through a series of parameter sensitivity studies (*22*). In this article, we show that Monte Carlo simulation results can be used to predict the formation of enzymatic DSBs in *E. coli* and Chinese hamster V79 and xrs5 cells after exposure to low-LET radiation. In a second test of the model, published experimental data on the induction of point mutations in the human *HPRT* (hypoxanthine guanine phosphoribosyl transferase) gene after exposure to low- and high-LET radiation are compared to model predictions. These comparisons are used to highlight the potential strengths and weaknesses of the model for the prediction of pathway-specific repair outcomes.

METHODS

Monte Carlo Damage Formation and Repair Simulations

Two separate Monte Carlo algorithms are used to simulate the formation and repair of DNA damage. The Monte Carlo damage simulation (MCDS) algorithm (*23*) is used to predict the initial yield and types of DNA damage formed by ionizing radiation, and the Monte Carlo excision repair (MCER) model (*22*) is used to simulate repair outcomes, such as correct repair, repair with a mutation (at least one base substitution), and conversion into a DSB. Here we briefly summarize the overall Monte Carlo scheme and discuss two key parameters that govern the production of enzymatic DSBs (N_{inh}) and mutations (φ_{Bd}) within the MCER model. The strategy used to consider the potential impact of pathway interactions on repair outcomes is also summarized.

The overall Monte Carlo scheme used to simulate the formation and repair of DNA damage proceeds on a cell-by-cell basis. That is, each Monte Carlo simulation represents the formation and repair of damage within one cell. A repair simulation begins by using the MCDS algorithm to generate the random number of damage configurations expected within the DNA of a cell. The number and spatial distribution of the damage configurations predicted by the MCDS algorithm are in reasonable agreement with those predicted by track-structure simulations (*23*). The MCDS-generated damage configurations are then superimposed over an actual nucleotide sequence or a random nucleotide sequence. Next, the MCER model is used to simulate the repair, misrepair and aborted excision repair of damage within the entire genome or within a specific region of the DNA. For a detailed description of the MCER model as well as additional discussion on the validity and limitations of the model, see ref. (*22*).

In the MCER model, the lesions forming a cluster are removed sequentially through repeated rounds of excision repair. The excision repair of a cluster begins by assuming that any of the constituent lesions has an equal chance of initiating the repair process. To better mimic the expected order in which the lesions are removed, additional criteria may be imposed on the random damage selection process. One such criterion occurs when BER of a damaged base is inhibited by the presence of a strand break in the opposite strand. The inhibitory effect is included in BER simulations by specifying an inhibition distance, N_{inh}, in base pairs (bp). That is, the repair of a damaged base is inhibited as long as a strand break is present in the opposite strand within N_{inh} bp. Once the strand break is repaired, the damaged base can be removed through another round of excision repair. The order in which the lesions forming a cluster are processed by BER is thus sensitive to the assumed value for N_{inh}. N_{inh} is also the key parameter that governs the production of enzymatic DSBs.

The MCER model includes mechanistic details specific to both the short- and long-patch BER pathways as well as the NER pathway, such as the selection of incision points and repair synthesis using a damaged or undamaged template. The probability that repair synthesis opposite a damaged template results in a base substitution is governed by the parameter φ_{Bd}. Setting φ_{Bd} to 0.75 is equivalent to the assumption that all four nucleotides are equally likely to be inserted opposite a damaged base. For a random base insertion process such as this, the correct base will be inserted on average one out of four times and the incorrect base will be inserted three out of four times. For values of φ_{Bd} smaller than 0.75, repair synthesis is biased toward correct repair. Repair is strongly biased toward base substitutions for values of φ_{Bd} larger than 0.75 ($\varphi_{Bd} = 1$ means a base substitution always occurs). When the template is undamaged, the MCER model assumes that a base substitution occurs approximately once for every 10^4 synthesized nucleotides in the SP BER pathway ($\eta_{SP} = 10^{-4}$) and once per 10^6 synthesized nucleotides in the LP BER and NER pathways ($\eta_{LP} = \eta_{NER} = 10^{-6}$).

Pathway interactions can be included in repair simulations by specifying probability distributions that quantify the relative contribution each pathway makes to the overall repair of DNA damage. Because of uncertainties associated with the processing of radiation-induced damage by the BER and NER pathways, model results are presented in terms of three simplified repair scenarios: (1) All lesions are processed by short-patch BER (SP BER), (2) all lesions are processed by long-patch BER (LP BER), and (3) all base damages are removed by NER and all strand breaks are removed by LP BER. The combined NER/LP BER repair scenario is postulated because of the lack of experimental evidence that NER can repair strand breaks, and thus either the SP BER or LP BER pathway must be involved in the repair of any cluster that includes a strand break.

Ratio of Enzymatic to Prompt DSBs

The combined MCDS/MCER simulations produce estimates of the yields of prompt and enzymatic DSBs per cell for a given radiation dose. All of the reported results are based on random nucleotide sequences that contain approximately 60% A-T pairs and 40% G-C pairs (see ref. *22*). A total of 10^7 and 10^5 repair simulations (each simulation is equivalent to one damaged cell) were performed for a 1-Gy dose of low-LET (4.5 keV electrons) and high-LET (3.31 MeV α particles) radiation, respectively. The α-particle energy is the same as the average energy of the source used in the study of Gulston *et al.* (*17*). The ratio of enzymatic to prompt DSBs is computed by dividing the average enzymatic DSB yield (Gy^{-1} $cell^{-1}$) by the average prompt DSB yield (Gy^{-1} $cell^{-1}$). Because the MCDS-predicted yield of prompt DSBs and other classes of damage is proportional to absorbed dose (*23*) and because repair outcomes predicted by the MCER model are proportional to the initial damage yield, the ratio of enzymatic to prompt DSBs is independent of dose.

Yields of Point Mutations in the Human HPRT Gene

To estimate the point mutation frequency (PMF) in the *HPRT* gene, we used the formula

$$\mathrm{PMF} = \delta(N_1 + N_2) + N_3. \quad (1)$$

Here N_1 is the number of prompt DSBs formed within the *HPRT* gene exons (Gy^{-1} $cell^{-1}$), N_2 is the number of enzymatic DSBs within the exons (Gy^{-1} $cell^{-1}$), N_3 is the number of base substitutions within the

TABLE 1
Experimental Results for the Formation of Enzymatic DSBs

Biological system	Radiation	Enzymatic DSBs: prompt DSBs	Reference
E. coli K-12	γ rays (^{137}Cs)	1.5[a]	(*9*)
E. coli	X rays (50 kVp)	~2[a]	(*14*)
V79 Chinese hamster cells	X rays (150 kVp)	0.8[a]	(*11*)
xrs5 Chinese hamster cells	γ rays (^{60}Co)	0.3[b]	(*17*)

[a] Unity was subtracted from the reported values to convert fold increase in the DSB yield to the ratio of enzymatic to prompt DSBs.

[b] Calculated from the reported values of 6 enzymatic DSBs Gy^{-1} cell^{-1} and 22.1 prompt DSBs Gy^{-1} cell^{-1}.

exons (Gy^{-1} cell^{-1}), and δ is the fraction of the (prompt or enzymatic) DSBs converted into point mutations. The Monte Carlo simulations provide estimates of N_1, N_2 and N_3. To relate these quantities to experimental observations for the expected number of point mutations within the *HPRT* locus, an estimate of δ is needed. This parameter can be estimated as follows.

The interaction of break ends associated with two different DSBs will generally form larger-scale chromosomal rearrangements (i.e. chromosome aberrations). Thus point mutations are likely to be formed only when break ends are rejoined with their correct partner. A study by Rothkamm and Löbrich (*24*) suggests that approximately 50% of the DSBs formed within the *HPRT* locus of human cells are rejoined correctly. The fraction of break ends that rejoin to the correct partner is independent of dose (*25*) and LET (*26*). If all of the correctly rejoined DSBs form point mutations, the fraction of the DSBs formed within the *HPRT* locus that are converted into point mutations is about 50%, i.e., $\delta = 0.5$.

To estimate N_1, N_2 and N_3, the single and clustered damages formed by a 1-Gy dose of radiation were generated using the MCDS algorithm (*23*) and placed at random locations within the DNA of a cell containing 6×10^9 bp. The characteristics of the human *HPRT* gene, such as nucleotide sequence, location and size of all nine exons, are known (*27*),[2] and the actual nucleotide sequence was used in this study. Next the MCER model was used to process all clusters (or isolated damages) that occur within the exons of the *HPRT* gene. For each repair simulation, the number of prompt DSBs, the number of enzymatic DSBs, and the number of clusters repaired with mutations (base substitutions) within the exons were tallied. Simulations were repeated 10^8 times to determine average event frequencies per unit absorbed dose per cell, i.e. N_1, N_2 and N_3. The statistical uncertainties associated with the estimated mutation frequency can be reduced by increasing the number of simulations. However, the number of simulations has no impact on the mean mutation frequency. The *HPRT* point mutation frequency was then computed using Eq. (1).

In experiments, the estimated mutation frequency is typically based on the number of mutations observed in cells that survive irradiation. The mutation frequency per surviving cell tends to increase linearly with absorbed dose, whereas the mutation frequency per irradiated cell increases in a linear fashion for lower doses and then starts to decrease at higher doses because of radiation-induced cell killing. In the Monte Carlo simulations, repair outcomes are tallied regardless of the ultimate fate of the cell. The key assumption implicit in this model simplification is that any degradation in the repair capacity of a dying cell occurs much later than the time needed to complete the processing of the radiation-induced damage. Because of this assumption, estimates of *HPRT* mutation frequency derived from Monte Carlo simulations are most appropriately interpreted as mutation frequencies per surviving cell.

[2] After the publication of the article, one nucleotide was added to the sequence. The corrected *HPRT* gene nucleotide sequence and location of exons can be obtained from http://www.ncbi.nlm.nih.gov/entrez/viewer.fcgi?db=nucleotide&val=184369 (NCBI Nucleotide database, accession number M26434).

TABLE 2
Ratios of Enzymatic to Prompt DSBs Predicted by the Monte Carlo Simulations

	Low-LET radiation (4.5 keV electrons)		High-LET radiation (3.31 MeV α particles)	
Repair scenario	$N_{inh} = 3$	$N_{inh} = 8$	$N_{inh} = 3$	$N_{inh} = 8$
SP BER	1.89	0.40	1.45	0.47
LP BER	1.93	0.48	1.49	0.60
NER/LP BER	2.61	2.61	1.86	1.86

RESULTS

Formation of Enzymatic DSBs

Table 1 shows experimental data on the yields of DSBs formed during repair processes expressed as ratios of enzymatic to prompt DSBs. Absolute DSB yields depend on the cell type and experimental conditions and may vary substantially between different data sets. Also, differences exist between measured and predicted DSB yields. For example, the MCDS algorithm predicts 45.5 prompt DSBs Gy^{-1} cell^{-1} in an average mammalian cell from low-LET radiation, whereas one of the studies used in the comparisons (*17*) reports 22.1 prompt DSBs Gy^{-1} cell^{-1} for hamster cells irradiated with ^{60}Co γ rays. The data shown in Table 1 are listed in terms of ratios of DSB yields instead of the absolute DSB yields to correct for the fact that absolute DSB yields are different among the different experimental data sets and among the measured and model-predicted values.

For comparison to the measured data, Table 2 shows model-predicted ratios for damage configurations representative of low-LET radiation (4.5 keV electrons). The ratios are reported for inhibition distances (N_{inh}) of 3 bp and 8 bp. Other parameters used in the MCER simulations are as listed in Table 1 in ref. (*22*). For the SP BER and LP BER repair scenarios, the ratio of enzymatic to prompt DSBs decreases as the inhibition distance increases. The ratio does not change in the NER/LP BER repair scenario because base damages that require the DNA incision step are repaired through NER in that scenario, and the MCER model assumes that DNA incision in the NER pathway cannot be inhibited. Experiments with *E. coli* suggest that an

inhibition distance of 3 bp is appropriate (*28*), and model predictions for N_{inh} = 3 bp are in good agreement with the measured data for *E. coli* reported in Table 1. For the SP BER and LP BER scenarios, an inhibition distance of 8 bp produces the ratios of 0.4–0.5 enzymatic DSBs per prompt DSB, which falls between the values of 0.3 and 0.8 determined in experimental studies for Chinese hamster xrs5 (*17*) and V79 (*11*) cells, respectively. The comparison of measured and model-predicted ratios of enzymatic to prompt DSBs for low-LET radiation suggests that an inhibition distance of about 8 bp is appropriate for these cell lines.

For high-LET radiation (3.31 MeV α particles), the model predicts a ratio of enzymatic to prompt DSBs of 0.47 for the SP BER repair scenario and 0.60 for the LP BER repair scenario (Table 2, results for N_{inh} = 8 bp). In contrast to the model predictions, Gulston *et al.* (*17*) found no evidence that enzymatic DSBs are created in V79-4 hamster cells irradiated with α particles with an average energy of 3.31 MeV. These investigators attribute the lack of evidence for enzymatic DSBs after α-particle irradiation to the increased complexity of the damage spectrum. That is, clustered damage sites produced by high-LET radiation are sufficiently complex to render them refractory to enzymatic conversion into DSBs (*17*). If this is indeed the case, the mechanisms postulated in the MCER model will need to be refined to account for additional cluster complexity effects.

Induction of Point Mutations in the Human HPRT Gene

The shaded regions in Fig. 1 show the range of point mutation frequencies per cell within the human *HPRT* gene calculated according to Eq. (1) with δ = 0.5 for low- and high-LET radiation. The lower bound on the shaded regions represents the limiting case when all lesions are processed by SP BER and repair synthesis is strongly biased toward correct repair despite damage in the repair template (φ_{Bd} = 0). The upper bound on the shaded regions represents the case when all lesions are processed by LP BER and base insertion opposite a damaged nucleotide is random (φ_{Bd} = 0.75). For reference, the dotted line represents the limiting case when all base damages are processed by NER and all strand breaks are processed by LP BER (i.e. the NER/LP BER scenario) and φ_{Bd} = 0.75. The model predictions shown in Fig. 1A are for 4.5 keV electrons. In Fig. 1B, the lower bound is based on damage configurations for 0.88 MeV protons [radiation with the lowest LET among experimental studies used in comparisons to the simulated data; ref. (*37*)] and the upper bound is based on damage configurations for a 3.26 MeV α particles [radiation with the highest LET used in ref. (*38*)]. Characteristics of DNA damage sites produced by these types of radiation as well as some results from *HPRT* simulation study are summarized in Table 3. Table 4 provides estimates of the model-predicted point mutation frequencies (Gy^{-1} $cell^{-1}$) for specific combinations of simulation parameters. All of the results shown in Fig. 1 as well as in Table 4 are for an inhibition distance of 8 bp, which we consider more appropriate for mammalian cells because of the comparisons of measured and model-predicted enzymatic-to-prompt DSB ratios (Tables 1 and 2).

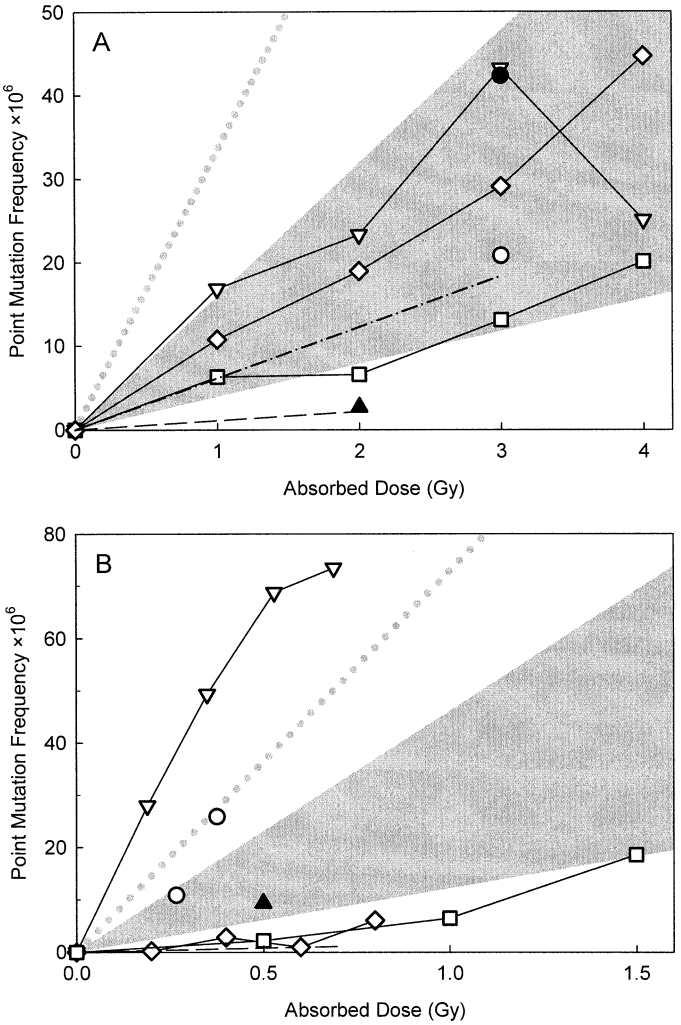

FIG. 1. Comparison of MCER simulation results (N_{inh} = 8 bp) and experimental data on the induction of radiation-induced point mutations in the human *HPRT* gene. Shaded regions indicate the range of model predictions for the BER pathways. Dotted lines show the upper bound on model-predicted point mutation frequency corresponding to a hypothetical NER/LP BER scenario. Symbols and lines show experimental data. Panel A: low-LET radiation (◇), ref. (*29*); (▲), ref. (*30*); (– – –), ref. (*31*) [the reported slope for the total mutation frequency (8.2×10^{-6} mutants/Gy) was scaled by the percentage of non-deletion type mutations (13%)]; (□), ref. (*32*); (▽), ref. (*33*); (○), ref. (*34*), Southern blotting; (●), ref. (*34*), multiplex PCR; (–·–), ref. (*35*) (the line is based on the reported slope of 6.11×10^{-6} mutants/Gy for point mutations). Panel B: high-LET radiation. (– – –), ref. (*31*) [the reported slope for the total mutation frequency (15.2×10^{-6} mutants/Gy) was scaled by the percentage of non-deletion type mutations (10%)]; (▽), ref. (*33*); (○), ref. (*34*); (◇), ref. (*36*); (□), ref. *37*; (▲), ref. (*38*). Experimental data points are connected by straight lines to guide the eye.

The data listed in Table 4 show that, for high-LET radiation, the point mutation frequency increases as particle

TABLE 3
Characteristics of DNA Damage Created by Different Types of Radiation as Predicted by the MCDS and MCER Models

Average value	4.5 keV electrons	0.88 MeV protons	3.26 MeV α particles
Number of clusters (Gy^{-1} $cell^{-1}$)	2.3×10^{3}	2.5×10^{3}	1.7×10^{3}
Number of damaged nucleotides per cluster	1.5	2.3	3.3
Cluster length (bp)	3.2	6.5	10.2
Number of clusters within the *HPRT* gene (Gy^{-1} $cell^{-1}$)[a]	2.2×10^{-2}	2.3×10^{-2}	1.6×10^{-2}
Number of clusters within exons (Gy^{-1} $cell^{-1}$)	2.6×10^{-4}	2.9×10^{-4}	2.1×10^{-4}
Number of prompt DSBs within exons (Gy^{-1} $cell^{-1}$)	5.4×10^{-6}	1.5×10^{-5}	2.1×10^{-5}

[a] The estimate is for the human *HPRT* gene with flanking regions (total length is 56,737 bp).

LET increases, as expected. Mutation frequencies for 3.26 MeV α particles are 2.2 to 3.6 times higher than mutation frequencies predicted for 4.5 keV electrons. The repair scenario and base misinsertion probability, φ_{Bd}, also have a substantial impact on the predicted point mutation frequencies for both low- and high-LET radiation. For example, the NER/LP BER repair scenario produces mutation frequencies that are about 2.5- to 4.5-fold higher than the corresponding mutation frequency for the SP BER pathway. The model-predicted point mutation frequencies increase 1.7- to 3.8-fold as φ_{Bd} increases from 0 (correct nucleotide is always inserted opposite a damaged base) to 0.75 (random nucleotide insertion opposite a damaged base).

Table 4 also shows the percentage contribution that δN_1, δN_2 and N_3 in Eq. (1) make to the total point mutation frequency. As a general trend, the model predicts that the contribution of the enzymatic DSBs becomes increasingly important compared to the contribution of the prompt DSBs in repair scenarios that have longer repair patches. The number of point mutations due to the N_3 term (base substitutions created during excision repair) is always larger for the LP BER and NER/LP BER scenarios than for SP BER. For the limiting case when the correct nucleotide is always inserted opposite a base damage ($\varphi_{Bd} = 0$), base substitutions arise from the spontaneous misinsertion of a non-complementary nucleotide opposite an undamaged template. The contribution of base substitutions (N_3) to the total point mutation yield in that case is negligible compared to the contributions of prompt (δN_1) and enzymatic (δN_2) DSBs.

For comparison to the Monte Carlo simulations, Fig. 1 shows measured data on point mutation yields in the human *HPRT* gene for several types of low- and high-LET radiation. The frequency of point mutations was obtained by multiplying the total yield of mutants at each dose by the fraction of mutants with point mutations at that dose. The mutant yields were corrected for spontaneous mutations by subtracting the background yield of cells with point mutations. The variability in the measured data apparent in Fig. 1 can be ascribed to a number of factors such as differences in radiation sources and dosimetry, variations in cell type and growth conditions, and the experimental method used to determine the mutation spectrum. For example, the data reported by Albertini *et al.* (*34*) were obtained for the same absorbed dose (3 Gy) using two different techniques to determine the mutation spectrum, i.e. Southern blotting and

TABLE 4
Effects of Parameters and Assumptions on Point Mutation Frequencies $\times 10^6$ (Gy^{-1} $cell^{-1}$) Predicted by the MCER Model (N_{inh} = 8 bp)

	Low-LET radiation[a]		High-LET radiation[b]	
Repair scenario	$\varphi_{Bd} = 0$	$\varphi_{Bd} = 0.75$	$\varphi_{Bd} = 0$	$\varphi_{Bd} = 0.75$
SP BER	3.9[c] (70, 30, 0)[d]	7.3 (35, 15, 50)	12.1[c] (66, 34, 0) 15.4 (68, 32, 0) 13.0 (62, 38, 0)	20.1 (38, 20, 42) 26.0 (40, 18, 42) 39.3 (20, 13, 67)
LP BER	4.1 (66, 34, 0)	15.9[c] (16, 9, 75)	16.7 (62, 38, 0) 25.1 (32, 68, 0)	46.1[c] (23, 14, 63) 72.2 (11, 24, 65)
NER/LP BER	10.0 (27, 73, 0)	33.3[e] (8, 22, 70)	29.3 (35, 65, 0)	72.8[e] (15, 25, 60)

[a] 4.5 keV electrons.

[b] The top value in each cell corresponds to the radiation type with the lowest LET used in experimental data selected for comparisons (0.88 MeV protons), and the bottom value is for the radiation type with the highest LET (3.26 MeV α particles).

[c] These values correspond to the lowest and the highest slopes of mutation frequency that define the shaded regions in Fig. 1.

[d] The values in parentheses are percentage contributions of δN_1, δN_2 and N_3 to the total point mutation frequency (Eq. 1).

[e] These values correspond to the slopes of dotted lines in Fig. 1.

multiplex PCR analysis. The estimate of point mutation frequency from PCR analysis is approximately twice the value determined using Southern blots.

The comparison of measured and model-predicted results in Fig. 1 demonstrates that, for both low- and high-LET radiation, the range of MCER model predictions overlaps substantially with the range of experimentally determined mutation yields. The mutation frequencies reported by Yamada *et al.* (*33*) for α particles cannot be explained by the model using any reasonable combination of parameters. However, Singleton *et al.* (*38*) measured mutation frequencies in cells of the same origin (human fibroblasts) using similar radiation types (3.26 MeV α particles and 3.5 MeV α particles, respectively), and their estimate of the mutation frequency at 0.5 Gy is severalfold lower and overlaps with the model predictions.

Ionizing radiation of high LET can produce non-random DSB distributions within the DNA [see ref. (*39*) for a review], and this implies that the distribution of other kinds of damage within the DNA may also be non-random. Large-scale (regional) clustering of damage may cause more hits to the *HPRT* locus of some cells, while in other cells damage sites will be clustered in different regions of the DNA and the *HPRT* locus will receive fewer hits. When these effects are averaged over a large number of cells, the resulting average number of hits and, consequently, the average number of mutations and DSBs in the *HPRT* gene exons are expected to be the same for both random and non-random damage induction mechanisms. We have verified this expectation using non-random damage distributions, and the simulation results presented in Fig. 1B do not change (data not shown).

DISCUSSION

For *E. coli*, the comparison between measured and model-predicted ratios of enzymatic to prompt DSBs for low-LET radiation suggests that an inhibition distance of 3 bp is appropriate. An inhibition distance of 8 bp gives good agreement with the available measured data for Chinese hamster cells. The trend in the inhibition distance suggested by this comparison is consistent with information reported in the literature for selected configurations of clustered damage. David-Cordonnier *et al.* (*40*) have investigated the processing of different classes of clustered damage by the *E. coli* BER enzymes Nth and Fpg and nuclear extracts from hamster cells. The results for a cluster composed of a damaged base, 5,6-dihydrothymine (DHT), opposite an AP site (AP sites are rapidly converted into strand breaks by AP endonucleases) showed that the inhibitory effect observed with mammalian nuclear extracts increases as the separation between the lesions increases from 1 to 5 bp (results for larger separation distances were not presented). This observation was in contrast to results obtained with bacterial glycosylases, which showed that the inhibitory effect decreases with the increasing separation between the two lesions.

Although the ratio of enzymatic to prompt DSBs predicted by the MCER model is in good agreement with data for Chinese hamster cells (*11, 17*), processes other than abortive excision repair (e.g. apoptosis, collapse of replication forks, etc.) may have contributed to the observed DSB yields (Table 1). Also, the xrs5 cell line used in the study of Gulston *et al.* (*17*) is defective in the p80 subunit of the Ku protein (*41*). Experiments (*42*) have shown that Ku can bind to nicked DNA opposite a dihydrouracil (DHU) and inhibit enzymatic DSB formation. The study by Hashimoto *et al.* (*42*) implicates the Ku protein in the repair of clustered DNA damage in addition to its known role in the non-homologous end joining (NHEJ) pathway and suggests that the formation of enzymatic DSBs in repair-proficient cells may be lower than that observed in the xrs5 (*17*) and TK6 (*18*) cell lines, which are both deficient in some aspects of DSB repair (*41, 43*). In repair-proficient human SC28 monocytes, Georgakilas *et al.* (*44*) found no evidence that enzymatic DSBs accumulate to detectable levels. However, the question of whether enzymatic DSBs are formed in repair-proficient cells remains open to debate because it is possible that enzymatic DSBs are repaired soon after they are formed and thus do not accumulate to significant levels in repair-proficient cells (*44*).

Within the MCER model, errors in DNA synthesis are assumed to yield single-base substitutions. Because of this model simplification, base substitutions cannot be distinguished from frameshift mutations or small deletions, even though BER polymerase β is known to create frameshifts when synthesizing past an AP site (*45, 46*). However, small-scale changes in DNA sequence (base substitutions, frameshift mutations, small deletions) are all categorized as point mutations (*19*) in experimental studies, and order-of-magnitude comparisons of the experimentally determined yields of point mutations to MCER simulation results are still appropriate.

The comparisons of measured and predicted values for the induction of point mutations in the human *HPRT* locus showed that the MCER model can reproduce the majority of experimental data, except for a few studies with both low- and high-LET radiation that produced low estimates of mutation frequency. The low mutation yields observed in some experiments cannot be reproduced with any reasonable combination of model parameters if 50% of the initial prompt and enzymatic DSBs formed within the *HPRT* locus are converted into point mutations (i.e., if $\delta = 0.5$). However, fits to the low mutation yields can be obtained with smaller values for δ (data not shown). In biophysical terms, the fidelity of DSB repair increases as δ decreases. Another possible explanation is that enzymatic DSBs are repaired with higher fidelity than prompt DSBs. In support of the latter hypothesis, Hashimoto *et al.* (*42*) have suggested that the involvement of the Ku70/80 complex in the repair of a clustered damage may provide op-

portunities to directly channel enzymatically formed DSBs into the NHEJ pathway, which in turn might increase the fidelity of DSB repair.

The reasonable agreement between the measured and predicted ratios of enzymatic to prompt DSBs (Tables 1 and 2) and the order-of-magnitude agreement between measured *HPRT* mutation frequencies and simulation results (Fig. 1) is encouraging, despite large uncertainties in the latter. To reduce uncertainties associated with model predictions, additional work is needed to identify the pathway or pathways involved in the repair of all classes of DNA damage other than DSBs. The model predicts that competition and regulation of the SP BER and LP BER pathways may produce up to a 20% difference in the ratio of enzymatic to prompt DSBs (Table 2) and a fourfold change in the point mutation frequency (Table 4). If NER is involved in the repair of clustered damages, pathway interactions may produce a sixfold change in the ratio of enzymatic to prompt DSBs and a fivefold change in the point mutation frequency. Uncertainties associated with the φ_{Bd} parameter also have a large effect on the model-predicted point mutation frequency (Table 4). These uncertainties arise because this parameter describes the aggregate effects of incorrect base insertion opposite many different types of base damage.

Although additional details of the excision repair process specific to the type of lesion (e.g. 8-oxoG, thymine glycol) can easily be incorporated into the Monte Carlo scheme, the models used to predict radiation-induced damage to DNA (*4*, *47*), including the MCDS algorithm (*23*) used as a source of damage configurations in this work, do not provide information about the yield of AP sites or specific types of base damage. The practical importance of many lesion-specific events and processes cannot be addressed until methods of predicting the yields of all types of radiation-induced DNA lesions become available. Additional experimental and theoretical work in this area is very desirable.

In the companion article (*22*), we proposed for the first time a quantitative Monte Carlo model that can be used to simulate the excision repair of DNA damage other than DSBs. As a first step toward testing the accuracy and validity of the MCER model, this article compares selected model predictions to measured data from the literature. The comparisons suggest that the MCER model can be used to quantify key end points related to the repair of oxidative DNA damage in selected bacterial and mammalian cell lines. As additional experimental data become available, the MCER model can be refined to improve the accuracy of model predictions and incorporate additional details of the clustered damage repair.

ACKNOWLEDGMENTS

This work is supported by the Office of Science (BER), U.S. Department of Energy, Grant Nos. DE-FG02–03ER63541 and DE-FG02–03ER63665.

Received: December 6, 2004; accepted: April 26, 2005

REFERENCES

1. J. F. Ward, DNA damage produced by ionizing radiation in mammalian cells: Identities, mechanisms of formation, and reparability. *Prog. Nucleic Acid Res. Mol. Biol.* **35**, 95–125 (1988).
2. J. F. Ward, Nature of lesions formed by ionizing radiation. In *DNA Damage and Repair*, Vol. 2 (J. A. Nickoloff and M. F. Hoekstra, Eds.), pp. 65–84. Humana Press, Totowa, NJ, 1998.
3. D. T. Goodhead, Initial events in the cellular effects of ionizing radiations: Clustered damage in DNA. *Int. J. Radiat. Biol.* **65**, 7–17 (1994).
4. H. Nikjoo, P. O'Neill, D. T. Goodhead and M. Terrissol, Computational modelling of low-energy electron-induced DNA damage by early physical and chemical events. *Int. J. Radiat. Biol.* **71**, 467–483 (1997).
5. B. M. Sutherland, P. V. Bennett, O. Sidorkina and J. Laval, Clustered DNA damages induced by X rays in human cells. *Radiat. Res.* **157**, 611–616 (2002).
6. M. Gulston, J. Fulford, T. Jenner, C. de Lara and P. O'Neill, Clustered DNA damage induced by γ radiation in human fibroblasts (HF19), hamster (V79-4) cells and plasmid DNA is revealed as Fpg and Nth sensitive sites. *Nucleic Acids Res.* **30**, 3464–3472 (2002).
7. S. S. Wallace, Enzymatic processing of radiation-induced free radical damage in DNA. *Radiat. Res.* **150** (Suppl.), S60–S79 (1998).
8. J. T. Reardon and A. Sancar, Molecular mechanism of nucleotide excision repair in mammalian cells. In *Advances in DNA Damage and Repair* (M. Dizdaroglu and A. Karakaya, Eds.), pp. 377–393. Kluwer Academic/Plenum Publishers, New York, 1999.
9. T. Bonura, K. C. Smith and H. S. Kaplan, Enzymatic induction of DNA double-strand breaks in γ-irradiated *Escherichia coli* K-12. *Proc. Natl. Acad. Sci. USA* **72**, 4265–4269 (1975).
10. D. L. Dugle, C. J. Gillespie and J. D. Chapman, DNA strand breaks, repair, and survival in x-irradiated mammalian cells. *Proc. Natl. Acad. Sci. USA* **73**, 809–812 (1976).
11. G. Ahnström and P. E. Bryant, DNA double-strand breaks generated by the repair of X-ray damage in Chinese hamster cells. *Int. J. Radiat. Biol.* **41**, 671–676 (1982).
12. Y. Ventur and D. Schulte-Frohlinde, Does the enzymatic conversion of DNA single-strand damage into double-strand breaks contribute to biological inactivation of γ-irradiated plasmid DNA? *Int. J. Radiat. Biol.* **63**, 167–171 (1993).
13. L. Harrison, Z. Hatahet and S. S. Wallace, *In vitro* repair of synthetic ionizing radiation-induced multiply damaged DNA sites. *J. Mol. Biol.* **290**, 667–684 (1999).
14. J. O. Blaisdell and S. S. Wallace, Abortive base-excision repair of radiation-induced clustered DNA lesions in *Escherichia coli*. *Proc. Natl. Acad. Sci. USA* **98**, 7426–7430 (2001).
15. B. Rydberg, Radiation-induced heat-labile sites that convert into DNA double-strand breaks. *Radiat. Res.* **153**, 805–812 (2000).
16. B. Stenerlöw, K. H. Karlsson, B. Cooper and B. Rydberg, Measurement of prompt DNA double-strand breaks in mammalian cells without including heat-labile sites: Results for cells deficient in nonhomologous end joining. *Radiat. Res.* **159**, 502–510 (2003).
17. M. Gulston, C. de Lara, T. Jenner, E. Davis and P. O'Neill, Processing of clustered DNA damage generates additional double-strand breaks in mammalian cells post-irradiation. *Nucleic Acids Res.* **32**, 1602–1609 (2004).
18. N. Yang, H. Galick and S. S. Wallace, Attempted base excision repair of ionizing radiation damage in human lymphoblastoid cells produces lethal and mutagenic double strand breaks. *DNA Repair* **3**, 1323–1334 (2004).
19. A. J. Grosovsky, J. G. de Boer, P. J. de Jong, E. A. Drobetsky and B. W. Glickman, Base substitutions, frameshifts, and small deletions constitute ionizing radiation-induced point mutations in mammalian cells. *Proc. Natl. Acad. Sci. USA* **85**, 185–188 (1988).

20. M. Weinfeld, A. Rasouli-Nia, M. A. Chaudhry and R. A. Britten, Response of base excision repair enzymes to complex DNA lesions. *Radiat. Res.* **156**, 584–589 (2001).

21. J. F. Ward, G. D. D. Jones and J. R. Milligan, Biological consequences of non-homogenous energy deposition by ionising radiation. *Radiat. Prot. Dosim.* **52**, 271–276 (1994).

22. V. A. Semenenko, R. D. Stewart and E. J. Ackerman, Monte Carlo simulation of base and nucleotide excision repair of clustered DNA damage sites. I. Model properties and predicted trends. *Radiat. Res.* **164**, 180–193 (2005).

23. V. A. Semenenko and R. D. Stewart, A fast Monte Carlo algorithm to simulate the spectrum of DNA damages formed by ionizing radiation. *Radiat. Res.* **161**, 451–457 (2004).

24. K. Rothkamm and M. Löbrich, Misrejoining of DNA double-strand breaks in primary and transformed human and rodent cells: A comparison between the HPRT region and other genomic locations. *Mutat. Res.* **433**, 193–205 (1999).

25. M. Löbrich, B. Rydberg and P. K. Cooper, Repair of x-ray-induced DNA double-strand breaks in specific *Not* I restriction fragments in human fibroblasts: Joining of correct and incorrect ends. *Proc. Natl. Acad. Sci. USA* **92**, 12050–12054 (1995).

26. M. Löbrich, P. K. Cooper and B. Rydberg, Joining of correct and incorrect DNA ends at double-strand breaks produced by high-linear energy transfer radiation in human fibroblasts. *Radiat. Res.* **150**, 619–626 (1998).

27. A. Edwards, H. Voss, P. Rice, A. Civitello, J. Stegemann, C. Schwager, J. Zimmermann, H. Erfle, C. T. Caskey and W. Ansorge, Automated DNA sequencing of the human HPRT locus. *Genomics* **6**, 593–608 (1990).

28. J. O. Blaisdell, L. Harrison and S. S. Wallace, Base excision repair processing of radiation-induced clustered DNA lesions. *Radiat. Prot. Dosim.* **97**, 25–31 (2001).

29. H. Kimura, H. Higuchi, H. Iyehara-Ogawa and T. Kato, Sequence analysis of X-ray-induced mutations occurring in a cDNA of the human *hprt* gene integrated into mammalian chromosomal DNA. *Radiat. Res.* **134**, 202–208 (1993).

30. S. L. Nelson, C. R. Giver and A. J. Grosovsky, Spectrum of X-ray-induced mutations in the human *hprt* gene. *Carcinogenesis* **15**, 495–502 (1994).

31. C. Y. Bao, A. H. Ma, H. H. Evans, M. F. Horng, J. Mencl, T. E. Hui and W. D. Sedwick, Molecular analysis of hypoxanthine phosphoribosyltransferase gene deletions induced by α- and X-radiation in human lymphoblastoid cells. *Mutat. Res.* **326**, 1–15 (1995).

32. M. S. Park, T. Hanks, A. Jaberaboansari and D. J. Chen, Molecular analysis of gamma-ray-induced mutations at the *hprt* locus in primary human skin fibroblasts by multiplex polymerase chain reaction. *Radiat. Res.* **141**, 11–18 (1995).

33. Y. Yamada, M. S. Park, R. T. Okinaka and D. J. Chen, Molecular analysis and comparison of radiation-induced large deletions of the *HPRT* locus in primary human skin fibroblasts. *Radiat. Res.* **145**, 481–490 (1996).

34. R. J. Albertini, L. S. Clark, J. A. Nicklas, J. P. O'Neill, T. E. Hui and R. Jostes, Radiation quality affects the efficiency of induction and the molecular spectrum of *HPRT* mutations in human T cells. *Radiat. Res.* **148** (Suppl.), S76–S86 (1997).

35. M. Mognato, P. Ferraro, S. Canova, G. Sordi, A. Russo, R. Cherubini and L. Celotti, Analysis of mutational effects at the *HPRT* locus in human G_0 phase lymphocytes irradiated *in vitro* with γ rays. *Mutat. Res.* **474**, 147–158 (2001).

36. N. F. Metting, S. T. Palayoor, R. M. Macklis, R. W. Atcher, H. L. Liber and J. B. Little, Induction of mutations by bismuth-212 α particles at two genetic loci in human B-lymphoblasts. *Radiat. Res.* **132**, 339–345 (1992).

37. M. Mognato, E. Bortoletto, P. Ferraro, L. Baggio, R. Cherubini, S. Canova, A. Russo and L. Celotti, Genetic damage induced by *in vitro* irradiation of human G_0 lymphocytes with low-energy protons (28 keV/μm): *HPRT* mutations and chromosome aberrations. *Radiat. Res.* **160**, 52–60 (2003).

38. B. K. Singleton, C. S. Griffin and J. Thacker, Clustered DNA damage leads to complex genetic changes in irradiated human cells. *Cancer Res.* **62**, 6263–6269 (2002).

39. K. M. Prise, M. Pinto, H. C. Newman and B. D. Michael, A review of studies of ionizing radiation-induced double-strand break clustering. *Radiat. Res.* **156**, 572–576 (2001).

40. M. H. David-Cordonnier, J. Laval and P. O'Neill, Clustered DNA damage, influence on damage excision by XRS5 nuclear extracts and *Escherichia coli* Nth and Fpg proteins. *J. Biol. Chem.* **275**, 11865–11873 (2000).

41. B. K. Singleton, A. Priestley, H. Steingrimsdottir, D. Gell, T. Blunt, S. P. Jackson, A. R. Lehmann and P. A. Jeggo, Molecular and biochemical characterization of *xrs* mutants defective in Ku80. *Mol. Cell. Biol.* **17**, 1264–1273 (1997).

42. M. Hashimoto, C. D. Donald, S. M. Yannone, D. J. Chen, R. Roy and Y. W. Kow, A possible role of Ku in mediating sequential repair of closely opposed lesions. *J. Biol. Chem.* **276**, 12827–12831 (2001).

43. H. H. Evans, M. Ricanati, M. F. Horng, Q. Jiang, J. Mencl and P. Olive, DNA double-strand break rejoining deficiency in TK6 and other human B-lymphoblast cell lines. *Radiat. Res.* **134**, 307–315 (1993).

44. A. G. Georgakilas, P. V. Bennett, D. M. Wilson, III and B. M. Sutherland, Processing of bistranded abasic DNA clusters in γ-irradiated human hematopoietic cells. *Nucleic Acids Res.* **32**, 5609–5620 (2004).

45. E. Efrati, G. Tocco, R. Eritja, S. H. Wilson and M. F. Goodman, Abasic translesion synthesis by DNA polymerase β violates the ''A-rule''. Novel types of nucleotide incorporation by human DNA polymerase β at an abasic lesion in different sequence contexts. *J. Biol. Chem.* **272**, 2559–2569 (1997).

46. S. S. Daube, G. Tomer and Z. Livneh, Translesion replication by DNA polymerase δ depends on processivity accessory proteins and differs in specificity from DNA polymerase β. *Biochemistry* **39**, 348–355 (2000).

47. W. R. Holley and A. Chatterjee, Clusters of DNA damage induced by ionizing radiation: Formation of short DNA fragments. I. Theoretical modeling. *Radiat. Res.* **145**, 188–199 (1996).